TecnoLógicas

Evaluation of Acoustic Excitation on the Stability and Thermal Performance of Nanofluids

Evaluación de excitación acústica en la estabilidad y desempeño térmico de nanofluidos

Juan José Alcalde Castro[1]; Laura Carolina Álvarez Gil[1,2]; Alejandro Restrepo-Martínez[1]

[1]Universidad Nacional de Colombia – Sede Medellín, Medellín, Colombia
[2]Institución Universitaria Pascual Bravo, Medellín, Colombia

Correspondence: jalcaldec@unal.edu.co

Received: 04 Abril 2025 **Accepted:** 21 January 2026 **Available:** 16 February 2026

How to cite / Cómo citar

J. J. Alcalde Castro, L. C. Álvarez Gil, and A. Restrepo-Martínez, "Evaluation of Acoustic Excitation on the Stability and Thermal Performance of Nanofluids," *TecnoLógicas*, vol. 29, no. 65, e3450, 2026.
https://doi.org/10.22430/22565337.3450

Abstract

Nanofluids with magnetic nanoparticles have been proposed to enhance heat transfer and energy conversion. However, the performance of these fluids depends on suspension stability and thermal distribution under irradiation. Low-frequency acoustic excitation emerges as an active strategy to modulate mixing and heat transport in these systems. The objective of this research was to determine the effect of low-frequency acoustic excitation on suspension stability, radiative absorption, and thermal efficiency of nanofluids containing magnetite nanoparticles (Fe_3O_4) dispersed at 0.05, 0.25, and 0.5% v/v in an ethylene glycol–water mixture. The methodology included exposing the nanofluids to acoustic waves generated by a loudspeaker while irradiating them with visible and infrared light from a halogen lamp. Stability was assessed through transmittance measurements, and thermal evolution and energy conversion were characterized using the specific absorption rate (SAR) and the stored energy ratio (SER). A comparison was made between different nanoparticle concentrations and excitation conditions. The results demonstrated that acoustic excitation influenced the stability and thermal distribution of the fluid. The extent of these effects varied depending on concentration and experimental conditions. In particular, excitation reduced thermal stratification and increased homogenization in certain cases, whereas in others it did not yield significant improvements in thermal efficiency (SAR/SER). Finally, it is concluded that when used in conjunction with an acoustic excitation system, nanofluids can be utilized more effectively in thermal applications because the acoustic excitation system promotes more uniform temperature fields.

Keywords

Acoustic wave, energy conversion, ferrofluid, nanoparticle, thermal energy.

Resumen

Los nanofluidos con nanopartículas magnéticas se han propuesto para mejorar la transferencia de calor y la conversión energética; sin embargo, su desempeño depende de la estabilidad de la suspensión y de la distribución térmica bajo irradiación. La excitación acústica de baja frecuencia se perfila como una estrategia activa para modular la mezcla y el transporte de calor en estos sistemas. El objetivo de esta investigación fue determinar el efecto de una excitación acústica de baja frecuencia sobre la estabilidad de la suspensión, la absorción radiactiva y la eficiencia térmica de nanofluidos con nanopartículas de magnetita (Fe_3O_4) dispersas a 0,05; 0,25 y 0,5 % v/v en una mezcla de etilenglicol y agua. La metodología empleada consistió en exponer los nanofluidos a ondas acústicas generadas por un altavoz mientras se irradiaban con luz visible e infrarroja de una lámpara halógena. La estabilidad se evaluó mediante medidas de transmitancia, y la evolución térmica y la conversión de energía se caracterizaron mediante la tasa de absorción específica (SAR) y la razón de energía almacenada (SER). Se compararon las distintas concentraciones de nanopartículas y las condiciones experimentales de excitación. Los resultados mostraron que la excitación acústica modificó la estabilidad y la distribución térmica del fluido, y la magnitud de los efectos dependió de la concentración y del régimen experimental. En particular, la excitación redujo la estratificación térmica e incrementó la homogeneización en ciertos casos, mientras que en otros no produjo mejoras significativas en la eficiencia térmica (SAR/SER). Finalmente, se concluye que la incorporación de un sistema de excitación acústica puede optimizar el desempeño de los nanofluidos en aplicaciones térmicas al favorecer campos de temperatura más uniformes.

Palabras clave

Onda acústica, conversión energética, ferrofluido, nanopartícula, energía térmica.

1. INTRODUCTION

Renewable energies have emerged as a sustainable solution, with solar energy representing a particularly promising avenue for mitigating environmental impacts and diversifying the energy matrix [1]-[4]. The installed capacity of solar energy, both photovoltaic and thermal, has undergone exponential growth over the last decade, establishing itself as an energy source with the highest projected participation in the generation in the energy transition process [5].

Solar energy is harnessed through direct conversion to electricity using photovoltaic systems and heat capture using solar thermal collectors, which are used to heat fluids for heating applications and industrial processes [6], [7]. In the latter category, direct-absorption solar collectors (DASC) are distinguished by their ability to absorb solar radiation directly into the working fluid, resulting in a rapid temperature increase and high thermal efficiency [5]. This advanced technology enhances the utilization of solar energy in applications that require constant heat, and it has established itself as a pivotal alternative in the transition to sustainable and efficient energy [8].

In Direct Absorption Solar Collectors (DASCs), the working fluids can range from common liquids, such as water, ethylene glycol, and oil, to advanced colloids, such as nanofluids [9]. The integration of nanoparticles into a base fluid not only markedly enhances the thermal and optical absorption characteristics of the fluid but also optimizes its thermal conductivity, thereby increasing the efficiency of direct absorption by solar collectors (DASCs) in solar energy harvesting [5], [10]. Several studies have employed magnetic fields in conjunction with magnetically responsive nanofluids, such as magnetite (Fe_3O_4) and maghemite (γ-Fe_2O_3) nanofluids, with the objective of further enhancing the thermal conductivity and efficiency of the heating process [11], [12]. However, the implementation of nanofluids presents challenges such as thermal stability and the tendency of nanoparticles to settle [13]. These factors must be optimized to enhance the performance of nanofluids in solar applications.

The settling of nanoparticles in working fluids alters their optical and thermal properties, which may subsequently reduce the efficiency of DASC systems. As the nanoparticles settle, the fluid loses its homogeneity, reducing its capacity to absorb and convert solar radiation into thermal energy in a uniform manner [11]. This lack of stability results in alterations to the transmittance and reflectance of the fluid, thereby impairing its capacity to capture energy. Furthermore, sedimentation affects the thermal conductivity of the fluid because the nanoparticles at the bottom cannot contribute to the transfer of heat throughout the volume of the fluid [14]. This results in the formation of zones with reduced thermal efficiency and a reduction in the

temperature of the working liquid. On the other hand, maintaining the quality of the nanoparticle suspension is relevant because it guarantees optimal performance in solar collectors and facilitates the advancement of nanofluid technologies for the development of practical solar applications [9].

The stability of nanofluids can be classified into two strategies: those associated with the formulation process and those related to operation. The formulation conditions include the use of surfactants such as some carboxylic acids, pH adjustment by the addition of acids or bases, and appropriate selection of agitation power [15]-[18]. These factors improve the initial fluid stability by preventing agglomeration and sedimentation. On the other hand, the operating conditions correspond to the regulation of flow regimes and external stimuli, aiming to keep nanoparticles in suspension and avoiding their sedimentation [19]. These combined approaches are crucial for maintaining the thermal and optical properties of nanofluids in advanced heat transfer applications.

In the design of DASCs, the use of dynamic magnetic fields is a key consideration among external stimuli. These are presented as an effective strategy to enhance convection in Fe_3O_4 nanofluids in solar collectors by inducing active motion in the fluid that facilitates energy transfer from the surface to the bottom of the collector [20], [21]. This active convection not only optimizes the capture of thermal energy but also reduces the sedimentation of nanoparticles, thereby promoting greater fluid stability and achieving higher thermal efficiency [22].

Similarly, the use of ultrasonic waves has been demonstrated to enhance the stability of nanofluids and influence the transfer of heat through the processes of cavitation and agitation, thereby promoting uniform mixing and preventing particle settling [23]. Moreover, lower-frequency acoustic waves exert beneficial effects on heat transfer processes, particularly in heat exchangers [24]. These effects can be attributed to the induction of fluid agitation and the enhancement of thermal efficiency through the reduction of sticking on transfer surfaces [25]. This phenomenon suggests a promising application in solar collectors, where the use of acoustic waves can prevent unwanted sedimentation, thereby optimizing the stability and thermal performance of nanofluids.

In particular, in systems where the nanofluids under examination are confined, low-frequency waves induce a slight agitation in the fluid, which increases the Nusselt number by improving circulation and thermal transport in the areas near the surfaces. Moreover, the implementation of these waves causes alterations in the drag and lift coefficients, which promote vortex shedding in the nanofluid [25]. This resulted in a more uniform heat distribution and the prevention of low-mobility fluid layers near the collector walls. The heat transfer is optimized and can be exploited in the design of DASC systems. Loudspeakers are of note in this context because they offer versatile control with accessible and cost-effective equipment. Furthermore, the induction of fluid motion through these signals can potentially enhance thermal efficiency, thereby opening new avenues for the development of advanced systems.

This study aims to analyze how applying a low-frequency acoustic field enhances the ability of a nanofluid (Fe_3O_4/EG-H_2O) to capture visible radiation energy. Specifically, it evaluates how variations in solid concentration, radiation, and mechanical waves influence the amount of captured energy converted into temperature. The experimental setup included an acoustical loudspeaker to agitate the fluid volume while exposing it to a visible-light radiation source, allowing for thermal monitoring of the sample. This setup provides a deeper understanding of how these operational variables affect the thermal performance of nanofluids, thereby helping to determine their potential applications in solar energy harvesting systems.

2. METHODOLOGY

2.1 Preparation of samples

The ethylene glycol (EG) used in this study was procured from Panreac. A solution of water and ethylene glycol (1:1) was prepared as the base fluid. Subsequently, the quantities required

for the preparation of 50 ml of nanofluids were determined at volumetric concentrations of 0.05%, 0.25%, and 0.5% Fe_3O_4, as defined in the review concerning the formulation of nanofluids applicable to solar collectors. Fe_3O_4 nanoparticles of diameter (50 to 100 nanometers) were used, and they were supplied by Merck.

The preparation of the suspensions involved calculating the necessary amounts of water, ethylene glycol, and Fe_3O_4 using the mixture rule. The calculations used the density and specific heat data from Table 1 to determine the required quantities (Table 2. After mixing the components, the process included 30 min of mechanical agitation, followed by 10 min of ultrasound homogenization at 400 W and 20 kHz using a TU-1000E4 (Xian Toption Instrument Co).

Table 1. The properties base used in the evaluation fluid. On the other hand, the properties calculated for the base fluid are based on the fluid rule of mixtures. Source: adapted from [26], [27].

Property	Unit	Water	Ethylene glycol	Water/EG 1:1	Fe_3O_4
Density	kg/m³	997	1115	1054	5200
Specific Heat	J/kg°C	4180	2430	3256	670

Table 2. The properties of the samples prepared and evaluated are calculated using equations (1) and (2); which are found as equations (3) and (4) of [26]. Source: own elaboration.

Magnitude		Unit	Sample			
			0%	0.05%	0.25%	0.5%
Liquid Volume	V_f	cm³	50	49	49	49
Particle Volume	V_p	cm³	0.00	0.025	0.125	0.25
Liquid Mass	m_f	g	52.800	52.904	53.318	53.836
Particle Mass	m_{np}	g	0.000	0.130	0.650	1.300
Nanofluid density	ρ_{nf}	kg/m³	1056	1058	1066	1077
Nanofluid-specific heat	Cp_{nf}	J/kg.°C	3256	3254	3248	3240

Table 2 presents the calculated properties for the evaluated samples, which varied according to the nanoparticle concentration. The density and specific heat are calculated using equations (1) and (2). In these equations, φ represents the percentage of the nanoparticle concentration, while ρ_{bf} and ρ_{np} indicate the density of the base fluid and nanoparticle, respectively. Similarly, $C_{p,bf}$ and $C_{p,np}$, correspond to the specific heats of the base fluid and nanoparticle, respectively [26].

$$\rho_{nf} = (1-\varphi)\cdot\rho_{bf} + \varphi\cdot\rho_{np} \quad [\mathrm{kg/m^3}] \tag{1}$$

$$C_{p,nf} = \frac{(1-\varphi)\cdot\rho_{bf}\cdot C_{p,bf} + \varphi\cdot\rho_{np}\cdot C_{p,np}}{\rho_{bf}} \quad [\mathrm{J/kg°C}] \tag{2}$$

2.2 Nanofluids characterization

An XRD spectrum was obtained to identify the crystalline phases in the sample using a PANalytical Aeris instrument (PANalytical B.V.) with Cu-Kα as the X-ray source. The particle morphology and size were analyzed using images acquired with a Thermo Fisher Scientific Scios 2 LoVac dual-beam field emission scanning electron microscope (FIB-FESEM).

The stability of the nanofluids was evaluated using an A721 spectrophotometer. The samples were subjected to mechanical agitation for 10 min and subsequently deposited into acrylic cuvettes. Transmittance data for wavelengths between 350 and 1000 nm were collected at 5-minute intervals over a 30-minute period.

2.3 Experimental set-up

The samples were subjected to a 10-minute agitation process. Twenty-five milliliters of nanofluids were deposited on a glass Petri dish with a circular cross-sectional area of $3x10^{-3}$ m². The Petri dish was affixed to a loudspeaker using plastic cable ties to facilitate contact and transmission of mechanical excitation to the fluid. Furthermore, the sample was subjected to visible infrared radiation generated by a 250 W-60 Hz infrared lamp light bulb and a flat convex concentrator lens.

Figure 1 illustrates the experimental setup used to study the effects of simulated radiation and mechanical waves on a sample containing Fe_3O_4 magnetite nanoparticles. The setup includes a Máxima infrared lamp with a concentrator that directs light onto a 25 mL sample with nanoparticle concentrations of 0.5%, 0.25%, and 0.05% v/v. The lamp was preheated with a voltage of 110 V, power of 250 W, and frequency of 60 Hz for 10 min before exposure to ensure stable irradiance. A SM206-SOLAR pyranometer measured the power and recorded 1000 W/m² when the incident surface was 16 cm from the sample. Temperature monitoring was performed using a UT325 thermometer multimeter with type K thermocouples positioned at two depths in the liquid, 7 mm apart and 3.5 mm from the sample surface, to track temperature evolution throughout the experiment. In addition, a mechanical wave generator loudspeaker configured at 200 Hz introduced vibrations into the sample.

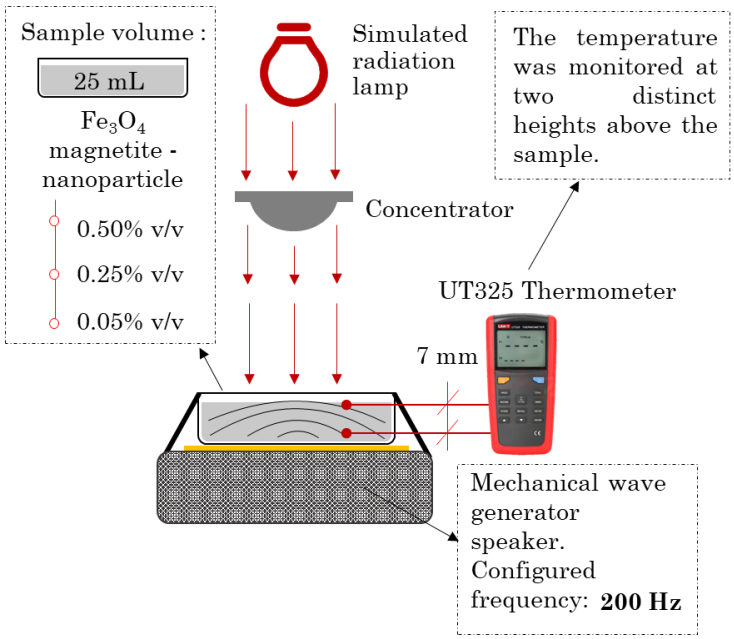

Figure 1. Experimental and instructions operatives of set-up. Source: own elaboration.

The experiment was conducted for a period of 10 min, during which the temperature of the two thermocouples was recorded at 60-s intervals. During this time, a 200-Hz and 45-dB square wave was generated by the loudspeaker. A frequency of 200 Hz and 45 dB used in the experiment were selected after oscillations were observed on the fluid surface, as shown in the subsequent results and discussion section. The surface oscillations indicate the generation of an agitation regime in the sample, which is associated with its composition and viscosity. This phenomenon suggests that the mechanical excitation at this frequency promotes forced convection in the nanofluid, thereby preventing the rapid sedimentation of the nanoparticles and homogenization in the thermal stratification of the sample.

2.4 Efficiency evaluation

To evaluate the performance of the heating system, the time evolution of the temperature was measured by the thermocouples. The temperature difference between the two thermocouples was calculated, as this provides information regarding the homogeneity of the thermal process of radiation transformation.

The specific absorption rate (SAR) and stored energy ratio (SER) were measured. The comparison between the SAR and SER values of different nanofluid formulations allows the determination of suspended solid concentrations that maximize the thermo-absorption effect. In addition, these indicators were used to evaluate operational variations due to the application of mechanical waves were analyzed, which allows evaluated whether of incident radiation transformed increases the internal energy in the nanofluid for the concentrations used.

The SAR is defined as the amount of energy captured by the nanofluid, normalized by the number of suspended solids present. This provides information about the efficiency of operating at a given concentration. The specific absorption rate (SAR) was calculated using the simplified mixing equation for a given nanofluid, as outlined in (3).

$$SAR = \frac{m_{nf} \cdot Cp_{nf} \cdot \overline{\Delta T_{nf}} - m_{bf} \cdot Cp_{bf} \cdot \overline{\Delta T_{bf}}}{m_{np} \cdot \Delta t} \qquad [W/kg_{np}] \tag{3}$$

The specific heat data and masses of the substances were calculated as simple mixture properties from the volumetric concentrations of water, EG, and Fe_3O_4 and are reported in Table 1. The change average temperature data, $\overline{\Delta T_{nf}}$ and ΔT_{bf} were the average of two thermocouples located in the fluid for each time interval Δt. Where $\overline{\Delta T_{nf}}$ is the sample corresponding to the nanofluid and $\overline{\Delta T_{bf}}$ is the sample corresponding to the base fluid. m_{np} is the mass in kilograms of the nanoparticles comprising the analyzed sample. Cp_{nf} and Cp_{bf} are the specific heats of the nanofluid samples, calculated based on their nanoparticle content and the specific heat of the base fluid, respectively, as shown in Table 1. The SAR is calculated temporally with a Δt=60 sec, in addition it is also calculated taking the whole experimental interval, which is Δt=600 sec.

The stored energy ratio SER, on the other hand, refers to the ratio of the energy stored by the nanofluid to the base fluid. The SER was calculated using the following in (4).

$$SER = \frac{\overline{T_{nf}}(t) - \overline{T_{nf}}(0)}{\overline{T_{bf}}(t) - \overline{T_{bf}}(0)} \qquad [\text{dimensionless}] \tag{4}$$

Where $\overline{T_{nf}}$ and $\overline{T_{bf}}$ represent the average temperatures of the nanofluid and base fluid at each time t, respectively. $\overline{T_{nf}}(0)$ and $\overline{T_{bf}}(0)$ being the temperature of the nanofluid and base fluid at time t=0.

3. RESULTS AND DISCUSSION

Figure 2 shows the XRD spectra. The identified peaks are consistent with those expected for pure Fe_3O_4 samples, where 30.13°, 35.50°, and 43.15° correspond to the (220), (311), and (400) diffraction planes, respectively, related to the inverse spinel crystal structure with a lattice parameter of 8.396 Å.

Figure 3 shows images of Fe_3O_4 nanoparticles captured using a field emission scanning electron microscope (FIB-FESEM). The nanoparticles exhibit a variety of shapes, including cubic and rounded forms, resulting in a range of particle sizes. The tendency of these nanoparticles to cluster together suggests that the nanofluids may exhibit low stability because of

gravitational effects acting on them. Furthermore, particles exceeding the size range specified by the supplier are evidenced, rendering them particularly susceptible to precipitation.

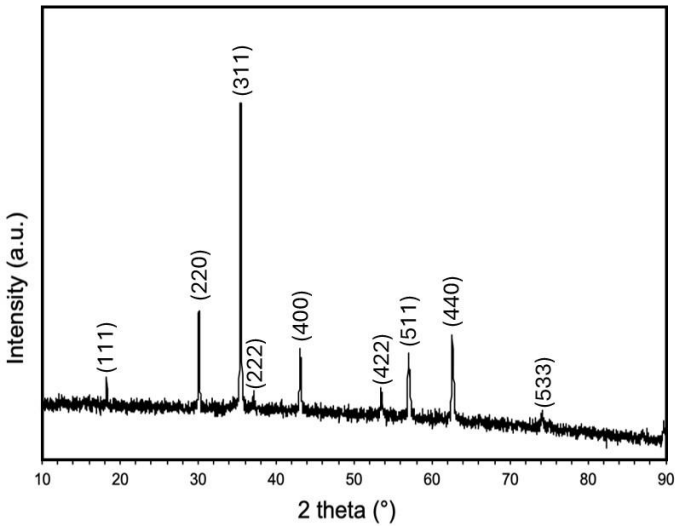

Figure 2. XRD analysis of Fe_3O_4. Source: own elaboration.

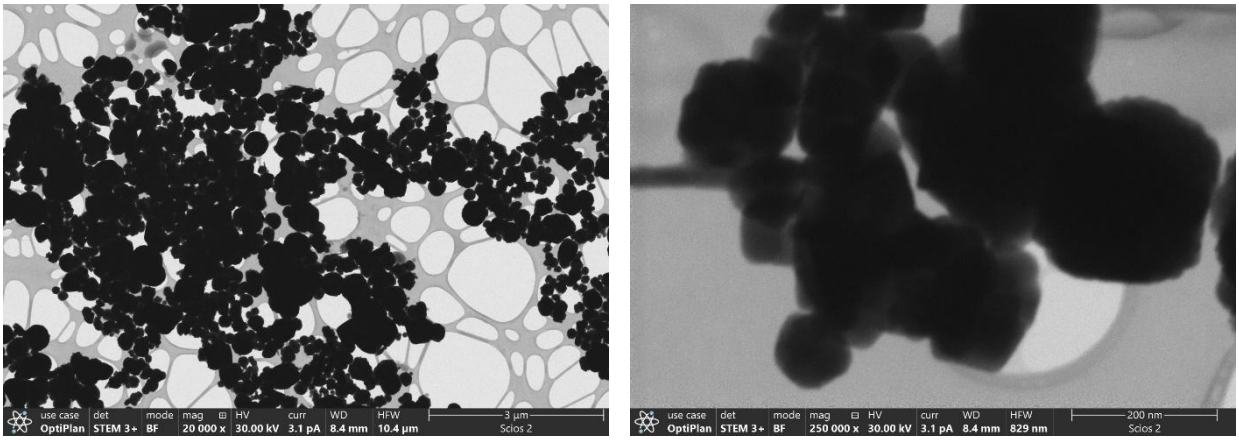

(a) (b)

Figure 3. FESEM images of Fe_3O_4: a) 20.000X b) 70.000X. Source: own elaboration.

Figure 4 shows a visual representation of the four samples that were subjected to evaluation: the 1:1 mixture of water and ethylene glycol, as well as the Fe_3O_4 nanofluids at concentrations of 0.05%, 0.25%, and 0.5% v/v, which were prepared in accordance with the parameters outlined in Section 2.1.

As illustrated in Figure 5a, the behavior of the analyzed fluids is demonstrated in the wavelength range 350–1020 nm. The EG/H_2O mixture maintains translucency across the entire spectrum, whereas the nanofluids at their three initial concentrations exhibit complete opacity to radiation within this range. Conversely, Figure 5b presents the time evolution of the transmittance at a wavelength of 550 nm, which was selected based on the reported transmittance peak for magnetite in the literature. The EG/H_2O mixture exhibited stable behavior over time, consistent with its homogeneous nature and resistance to degradation.

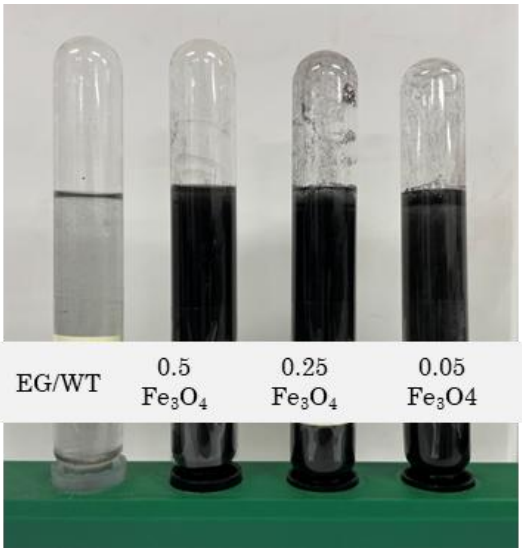

Figure 4. Appearance of the fluids used. Note: Samples were shaken for 10 min before imaging. Source: own elaboration.

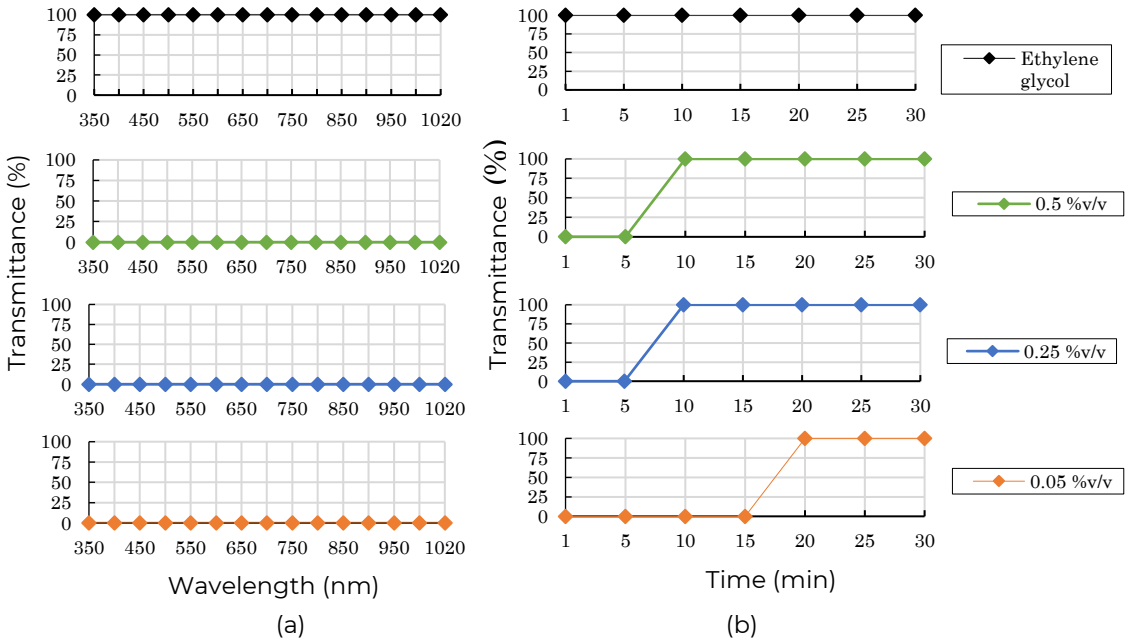

Figure 5. Transmittance measurement in the visible spectrum. a) Transmittance measurement for the samples in the first minute; b) Time evolution of the transmittance values for the samples at a wavelength of 550 nm. Source: own elaboration.

Conversely, nanofluids with concentrations of 0.5% and 0.25% v/v exhibit increased transmittance, reaching 100% between 5 and 10 min of analysis. The sample containing 0.05% v/v suspended solids also reached its maximum transmittance value, although in a longer time interval, approximately between 15 and 20 min.

The results presented in Figure 5 demonstrate the temporal stability of the EG/H_2O solution and the precipitation tendency of the evaluated nanofluids. Furthermore, it is evident that the nanofluid with 0.05% v/v demonstrates a slower sedimentation rate than those with 0.5% and 0.25% v/v, indicating enhanced stability in suspension during the initial minutes of the experiment.

The application of mechanical waves to materials generates distinct patterns. Such phenomena are known as Faraday instability and Chladni figures in the context of liquid and metallic plates [28]. When a sound wave is applied to a fluid from below, the focus is on the surface topography generated by the applied frequency and the arrangement of suspended or settling particles. Figure 6 shows some images corresponding to this phenomenon, and they illustrate the relationship between the surface pattern and the frequency of excitation of the applied sound wave, density of the fluid, and shape of the disk. Three samples were prepared: (a) pure ethylene glycol, (b) a mixture of ethylene glycol and water at a 1:1 ratio, and (c) a nanofluid at a concentration of 0.5% v/v Fe_3O_4. They were subjected to mechanical waves.

Figure 6. Vibration pattern associated with the sample composition. a) Pure ethylene glycol; b) EG/H2O. c) EG/H_2O 0.5% v/v Fe_3O_4 Nanofluid. Source: own elaboration.

Figure 6 illustrates the vibration patterns of different sample compositions subjected to mechanical waves. The samples include (a) pure ethylene glycol, (b) an ethylene glycol/water mixture, and (c) an ethylene glycol/water-based nanofluid containing 0.5% v/v Fe_3O_4 nanoparticles. The experiment used a mechanical wave generator loudspeaker configured at 200 Hz and 45 dB. Due to the high viscosity of pure ethylene glycol (Figure 6a), this frequency was insufficient to disrupt the surface equilibrium, resulting in the absence of a visible pattern. However, in Figures 6b and 6c, where the base fluid is a mixture of ethylene glycol and water, the reduction in viscosity facilitated the appearance of the Faraday instability, resulting in the formation of distinct surface patterns. This phenomenon was further influenced by Fe_3O_4 nanoparticles in the nanofluid.

The excitation of the fluid depends on its composition; a decrease in the surface excitation pattern is observed in the sample with nanofluid, due to the addition of nanoparticles with respect to the ethylene glycol/water fluid base, as can be seen in Figures 5b, c). The relationship between the excitation source and the vessel must be a fixed junction so that the mechanical wave can be transmitted to the fluid, which is the only one free to move. On the other hand, generating mechanical waves also introduces the presence of a magnetic field during its operation. This produces clusters of nanoparticles due to their magnetization, leading to particle aggregation and sedimentation, which negatively affects radiation absorption and, consequently, energy transformation.

Figure 7 illustrates the temporal thermal behavior of the evaluated samples, demonstrating the thermal performance of the two thermocouples at varying heights, as outlined in Section 2.3. Expected during agitation of the fluid, an increase in the bottom part and a decrease in the top part to homogenize the temperature of the sample.

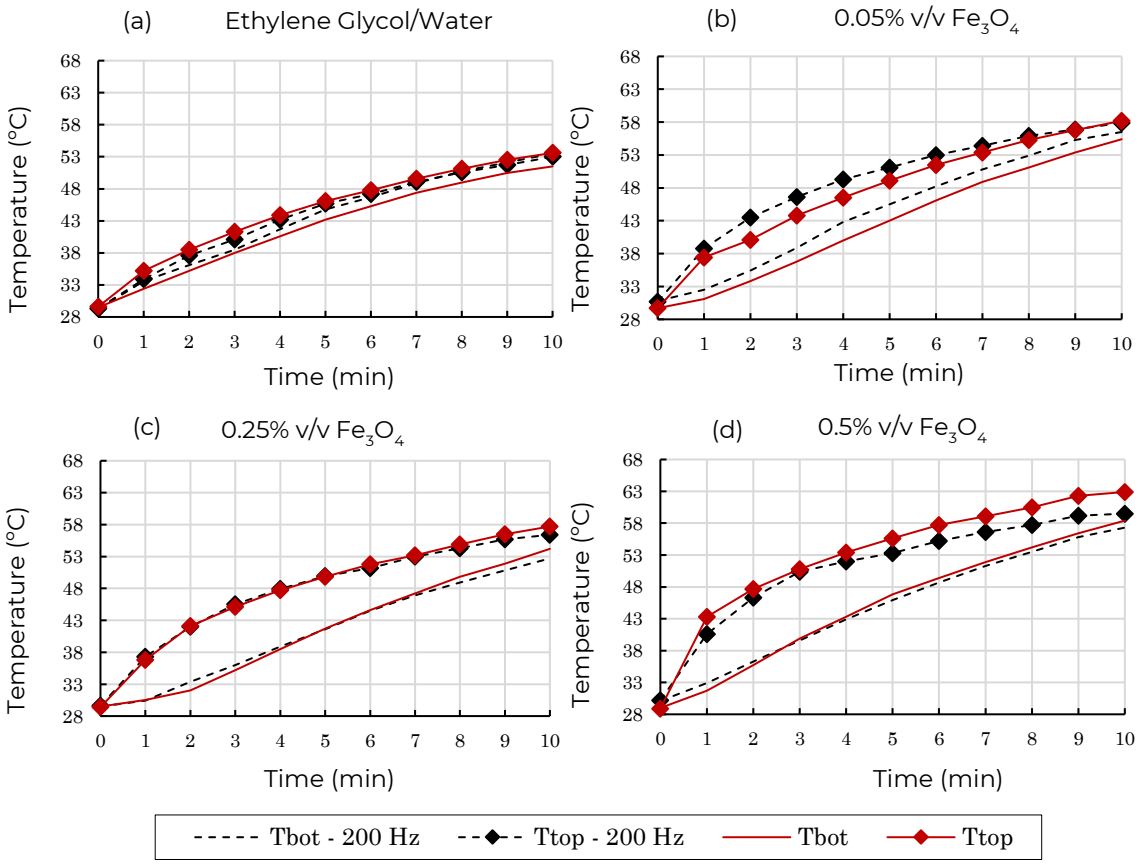

Figure 7. Temporal evolution of the temperature for the two thermocouples located at different heights: a) temporal evolution of the temperature for the ethylene glycol/water sample; b) temporal evolution of the temperature for the 0.05% Fe_3O_4 sample; c) temporal evolution of the temperature for the 0.25% Fe_3O_4 sample; and d) temporal evolution of the temperature for the 0.5% Fe_3O_4 sample. Source: own elaboration.

If a fluid does not exhibit variations in its optical properties, its heating will remain homogeneous regardless of its thickness. However, if the fluid is slightly transparent in the visible spectrum, the upper layers absorb more radiation and reach higher temperatures.

In a stratified fluid, agitation generates currents that promote particle movement, allowing all particles to reach the upper layers and receive, on average, the same amount of radiation. This resulted in a more uniform heat distribution throughout the fluid volume.

Based on these ideas, the results in the figure support this explanation. Figure 7(a) shows that ethylene glycol reached similar temperatures at both measurement positions. Additionally, agitating the sample at 200 Hz reduced the temperature difference. These observations indicate that ethylene glycol acts as a transparent fluid and achieves homogenization during heating, with the applied agitation further enhancing this process.

In Figures (b-d), the upper and lower temperatures differ in all cases, indicating a stratification process. The presence of nanoparticles alters the fluid's optical properties, having this effect. Additionally, the final temperature was varied by the nanoparticle volume fraction.

Regarding the effect of agitation, Figure 7(b) shows that the agitated fluid reaches a higher temperature than the reference sample. In Figure 7(c), both tests yield similar results. In Figure 7(d), the top temperature of the agitated sample is lower than that of the reference sample, suggesting reduced stratification after 5 min. However, particle precipitation, which increases over time and is particularly relevant for samples with a 0.5-volume fraction, could

also explain this effect. Finally, the applied agitation frequency did not significantly improve the temperature homogenization.

Figure 8 shows the evolution of the temperature difference (ΔT) between the upper and lower parts of the samples over time, considering the presence and absence of an excitation frequency of 200 Hz. In general, the temperature difference reaches a maximum around 3-4 minutes and then gradually decreases, indicating a tendency toward thermal equilibrium. Nanofluids with Fe_3O_4 concentrations show higher temperature differences compared to the base fluid (EG/H_2O), with the 0.5% v/v sample showing the highest ΔT. Furthermore, the application of the 200 Hz frequency tends to reduce the temperature difference in all cases, suggesting that mechanical excitation promotes thermal homogenization within the fluid.

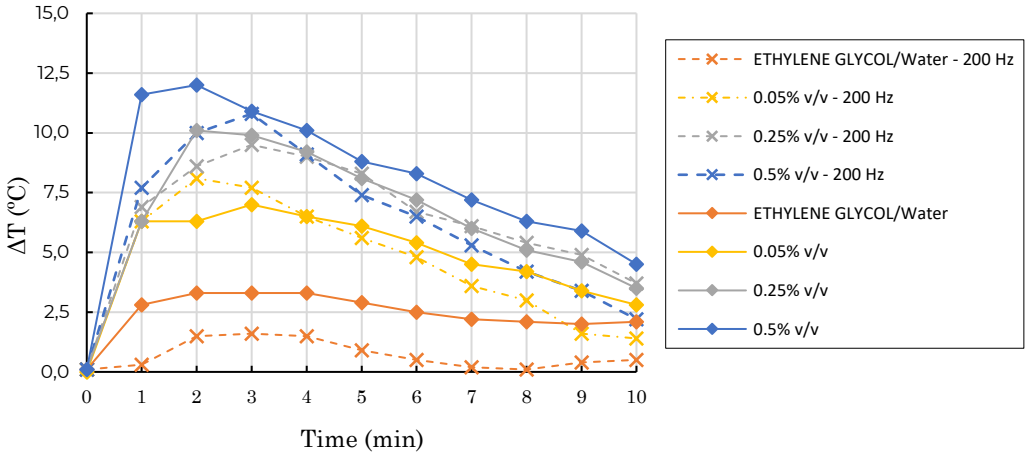

Figure 8. Difference between the upper and lower temperatures of the samples evaluated for the presence and absence of the excitation frequency. Source: own elaboration.

The sample that exhibited minimal thermal stratification when using the loudspeaker was ethylene glycol-water, a phenomenon that persisted throughout the evaluation period. In the 0.05% concentration, the effect of the loudspeaker on thermal stratification was noticeable after four minutes. In the 0.25% sample, thermal behavior exhibited a high degree of similarity under both conditions, with and without the loudspeaker. The 0.5% concentration exhibited the most pronounced stratification in the absence of a loudspeaker. The thermal difference among the samples decreases over time.

The 0.5% v/v sample showed the most pronounced thermal stratification without the loudspeaker, reaching the highest temperature difference at the start of the test. However, applying acoustic excitation at 200 Hz gradually reduced stratification throughout the experiment, except at minute three, where the thermal change remained similar. These findings suggest that acoustic excitation directly influences thermal stratification, with stronger effects appearing in the 0.0% and 0.05% v/v samples.

Figure 9a shows the evolution of the Specific Absorption Rate (SAR) over time for different concentrations of Fe_3O_4 nanoparticles (0.05%, 0.25%, and 0.5% v/v) under conditions with and without acoustic excitation (200 Hz). The y-axis represents the SAR values ($W/kgFe_3O_4$), while the x-axis corresponds to the time in minutes. The results show that the nanoparticle concentration significantly affects the thermal behavior of nanofluids. In particular, the lowest volume fraction (0.05% v/v) exhibited the highest SAR values, which is consistent with the definition of SAR as the energy absorbed per unit mass of nanoparticles. As the total mass of solids decreases, the energy absorbed per particle is relatively higher. Conversely, as the concentration increases (0.25% and 0.5% v/v), the specific yield decreases, resulting in a decrease in SAR values, as shown in Figure 10a. In addition, the data show that SAR tends to be higher in the absence of acoustic excitation, further supporting the observation that sound

waves do not enhance energy absorption under the conditions studied and may even contribute to a reduction in SAR.

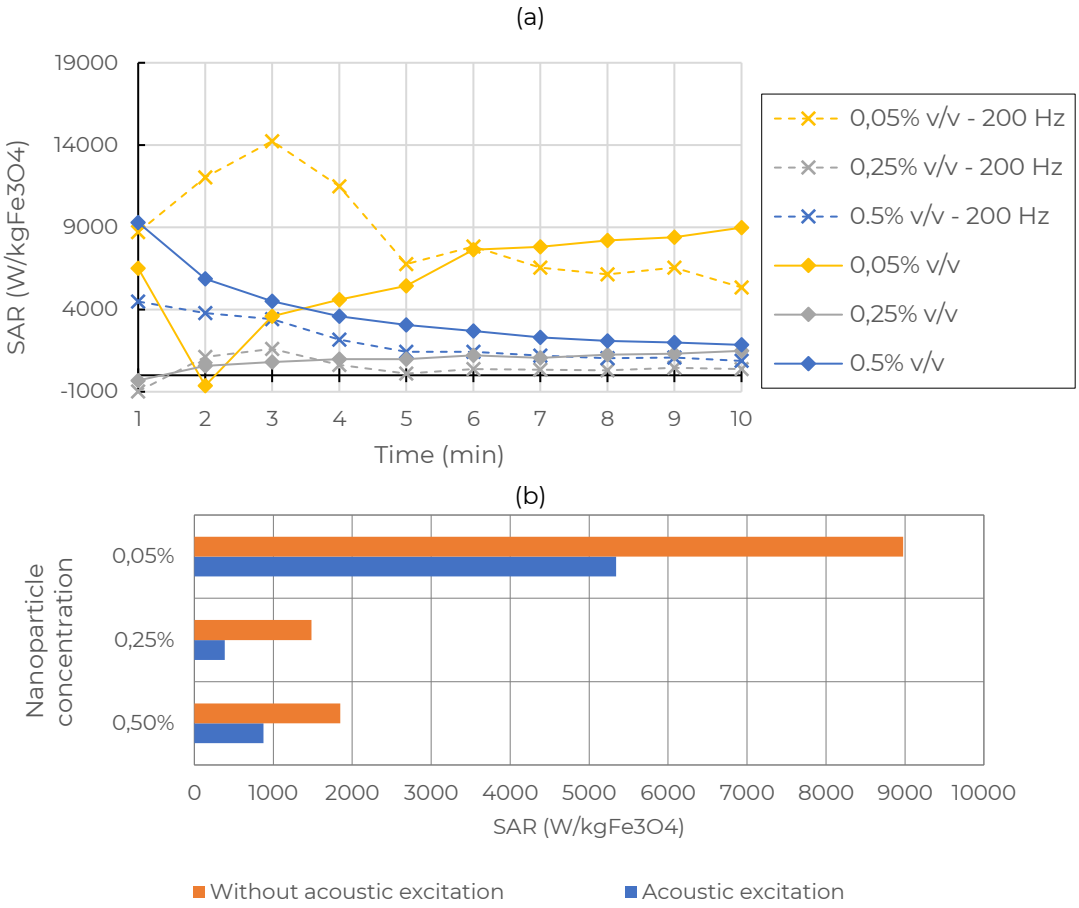

Figure 9. Indicators of the thermal behavior of the analyzed fluid: a) Temporal SAR and b) SAR at Δt=600 s. Source: own elaboration.

Figure 9b shows the Specific Absorption Rate (SAR) for different concentrations of Fe_3O_4 nanoparticles (0.05%, 0.25% and 0.5% v/v) under two conditions: without acoustic excitation (orange) and with acoustic excitation (blue). The results show that for all concentrations evaluated, the SAR is higher without acoustic excitation, with the most notable difference observed at 0.05% v/v. As the nanoparticle concentration increased (0.25% and 0.5% v/v), the SAR values decreased under both conditions, and the effect of acoustic excitation became even less pronounced. Although theoretical models suggest that sound waves enhance nanoparticle dispersion and heat transfer, the experimental results show the opposite effect under the specific frequency and amplitude conditions investigated in this study. This suggests that in this setup, acoustic excitation does not improve energy absorption efficiency and may even contribute to the reduction in SAR.

The Figure 10 shows the evolution of the SER (Signal Enhancement Ratio) over time (in minutes) for different Fe_3O_4 concentrations (0.05% v/v, 0.25% v/v, and 0.5% v/v) under with and without acoustic excitation at 200 Hz. The y-axis represents the SER value in dimensionless units (di), and the x-axis represents the elapsed time.

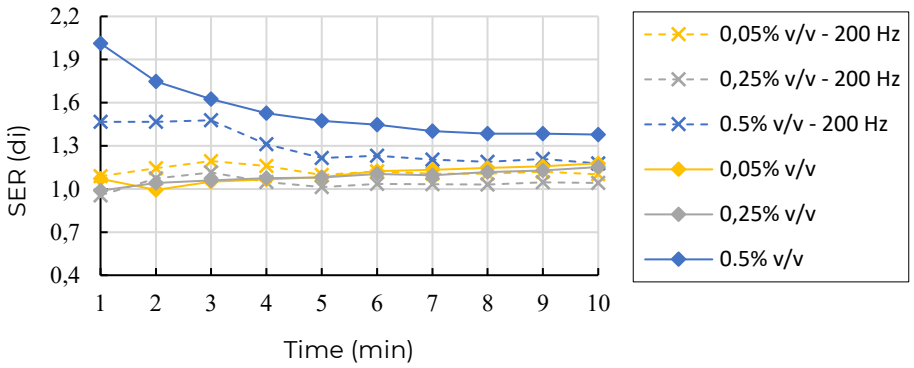

Figure 10. Indicators of the thermal behavior of the analyzed fluid, SER.
Source: own elaboration.

The results showed that 0.5% v/v concentration had the highest SER values, with a decreasing trend over time. Conversely, this concentration provided the optimal SER regardless of the presence or absence of acoustic excitation. In contrast, the 0.05% and 0.25% v/v concentrations showed more stable values, remaining close to one, with slight variations. Specifically, for the 0.25% v/v concentration under acoustic excitation, the SER remained close to unity throughout the evaluated time. In addition, for the 0.05% v/v concentration, no differences in SER values were observed between the conditions with and without the loudspeaker.

Furthermore, the presence of acoustic excitation at the lowest concentration (0.05% v/v - 200 Hz) did not seem to significantly increase the SER compared with the non-excitation condition. Taken together, these results suggest that a higher nanoparticle concentration initially promotes a higher SER, but over time, it tends to stabilize.

In the overall experiment, low-frequency acoustic excitation did not yield a consistent improvement in thermal efficiency, so a global performance increase cannot be claimed. However, an early advantage was observed: during the first 5 minutes, the excited samples showed a higher initial SAR. Therefore, it is advisable to assess efficiency using time-windowed metrics that capture time-dependent effects.

This work presents a simplified and replicable experimental setup that integrates optical stability and thermal performance under visible and infrared irradiation. This setup enables simultaneous evaluation of stratification and efficiency during audible excitation. The results indicate that excitation reduces stratification and facilitates thermal homogenization, with a dependence on concentration, though without consistently leading to overall improvements.

While the study demonstrates the viability of the approach, there are limitations that can be addressed: the use of a single frequency-amplitude set, along with a confined geometry, is a contributing factor. Additionally, colloidal stability was found to be restricted, which has the potential to influence efficiency estimates. Similarly, the presence of a magnet in the loudspeaker could impact measurements due to attraction or aggregation effects. These constraints can be mitigated by using the same setup with a systematic sweep of frequency and amplitude, comparing cell vs. flow configurations, and using nanofluids with greater temporal stability or alternative compositions. Ideally, the loudspeaker would be replaced with a piezoelectric actuator to more comprehensively determine how these factors affect thermal performance.

In contrast with other reports, which demonstrate significant improvements in transfer and system efficiency through the use of rotating magnetic fields or ultrasound in regimes with strong cavitation [29], [30], these findings indicate that audible excitation primarily reduces stratification and improves uniformity, though it does not consistently enhance overall efficiency. The findings of this study, when considered in conjunction with existing literature, indicate that the net benefit is contingent on several factors. These include the excitation

regime, characterized by frequency and intensity. The study also considers the hydrodynamic and thermal state of the test, the initial stability of the nanofluid, and the temporal scale of evaluation. [31]-[33]. It is noteworthy that under certain configurations, the acoustic input can result in mixing and uniformity, and in some cases, fluid–field coupling can enhance efficiency. These performance differences are consistent with forced-convection mechanisms and their sensitivity to flow regimes and transported heat [34]-[36]. However, the proposed approach enables a simple setup with which to implement changes in the convective processes of the nanofluids analyzed.

4. CONCLUSIONS

The transmittance results in the visible spectrum demonstrate that formulations with 0.25% and 0.5% v/v concentrations of Fe_3O_4 exhibit rapid sedimentation, reaching 100% transmittance in less than 10 min, indicating a significant loss of stability. Conversely, the sample with 0.05% v/v exhibited enhanced resistance to sedimentation, retaining its opacity for a longer period.

The specific absorption rate (SAR) analysis indicated that the formulation with 0.05% v/v Fe_3O_4 exhibited the highest thermal energy conversion efficiency, whereas at higher concentrations, a decrease in the relative efficiency was observed. Furthermore, the application of acoustic waves at 200 Hz and 45 dB did not significantly improve the temperature reached by the fluid, suggesting that the effectiveness of mechanical excitation depends on the concentration of nanoparticles and the properties of the system. These findings highlight the importance of adjusting excitation conditions to optimize heat transfer in nanofluids used in solar collection systems.

Future studies should use nanofluids with greater stability and minimal variation in viscosity with temperature to isolate and evaluate the effect of acoustic excitation on thermal performance.

5. ACKNOWLEDGMENTS

This work was also financed by the project “RC-2022-0766 - MINCIENCIAS - Diseño de un sistema de calentamiento complementario por inducción magnética termosolar, con uso nanosuspensiones desarrolladas a partir de materiales de procesamiento minero - H:51691”. In addition, this research was supported by the BEDA program of the Universidad Nacional de Colombia – Sede Medellín.

6. REFERENCES

[1] M. Yavari, and I. M. Bohreghi, “Developing a green-resilient power network and supply chain: Integrating renewable and traditional energy sources in the face of disruptions,” *Appl. Energy*, vol. 377, Part C, p. 124654, Jan. 2025. https://doi.org/10.1016/j.apenergy.2024.124654

[2] L. G. Tapia Carpio, and F. A. Cardoso Guimarães, “Regional diversification of hydro, wind, and solar generation potential: A mean-variance model to stabilize power fluctuations in the Brazilian integrated electrical energy transmission and distribution system,” *Renev. Ener.*, vol. 235, p. 121266, Nov. 2024. https://doi.org/10.1016/j.renene.2024.121266

[3] M. Becerra-Fernandez, A. T. Sarmiento, and L. M. Cardenas, “Sustainability assessment of the solar energy supply chain in Colombia,” *Energy*, vol. 282, p. 128735, Nov. 2023. https://doi.org/10.1016/j.energy.2023.128735

[4] J. Wang, and W. Azam, “Natural resource scarcity, fossil fuel energy consumption, and total greenhouse gas emissions in top emitting countries,” *Geoscience Front.*, vol. 15, no. 2, p. 101757, Mar. 2024. https://doi.org/10.1016/j.gsf.2023.101757

[5] A. Hasan, A. Alazzam, and E. Abu-Nada, "Direct absorption solar collectors: Fundamentals, modeling approaches, design and operating parameters, advances, knowledge gaps, and future prospects," *Prog. Energy Combust. Sci.*, vol. 103, p. 101160, Jul. 2024. https://doi.org/10.1016/j.pecs.2024.101160

[6] L. A. Omeiza *et al.*, "Application of solar thermal collectors for energy consumption in public buildings – An updated technical review," *J. Eng. Res.*, vol. 12, no. 4, pp. 994-1010, Dec. 2024. https://doi.org/10.1016/j.jer.2023.09.011

[7] A. Zaidi, "A bibliometric analysis of machine learning techniques in photovoltaic cells and solar energy (2014–2022)," *Energy Rep.*, vol. 11, pp. 2768-2779, Jun. 2024. https://doi.org/10.1016/j.egyr.2024.02.036

[8] M. Sainz-Mañas, F. Bataille, C. Caliot, A. Vossier, and G. Flamant, "Direct absorption nanofluid-based solar collectors for low and medium temperatures. A review," *Energy*, vol. 260, p. 124916, Dec. 2022. https://doi.org/10.1016/j.energy.2022.124916

[9] T. Gunay, C. Gumus, and A. Z. Sahin, "The impact of using nanofluid on the performance of solar stills: A comprehensive review," *Process Saf. Environ. Prot.*, vol. 189, pp. 1464-1516, Sep. 2024. https://doi.org/10.1016/j.psep.2024.06.104

[10] J. J. Alcalde-Castro, L. Álvarez-Gil, and A. Restrepo-Martínez, "Evaluation of the thermal efficiency of ethylene glycol/magnetite nanofluids for use in direct absorption solar collectors," in *Proceed., Nonimaging Optics: Efficient Design for Illumination and Concentration XIX*; San Diego, Cali, USA, Oct. 2024, vol. 13132, pp. 102-109. https://doi.org/10.1117/12.3028098

[11] M. Gürdal, K. Arslan, E. Gedik, and A. A. Minea, "Effects of using nanofluid, applying a magnetic field, and placing turbulators in channels on the convective heat transfer: A comprehensive review," *Renew. Sustain. Energy Rev.*, vol. 162, p. 112453, Jul. 2022. https://doi.org/10.1016/j.rser.2022.112453

[12] T. B. Gorji, and A. A. Ranjbar, "A review on optical properties and application of nanofluids in direct absorption solar collectors (DASCs)," *Renew. Sustain. Energy Rev.*, vol. 72, pp. 10-32, May. 2017. https://doi.org/10.1016/j.rser.2017.01.015

[13] Z. Said *et al.*, "Recent advances on the fundamental physical phenomena behind stability, dynamic motion, thermophysical properties, heat transport, applications, and challenges of nanofluids," *Phys. Rep.*, vol. 946, pp. 1-94, Feb. 2022. https://doi.org/10.1016/j.physrep.2021.07.002

[14] M. A. García-Rincón, and J. J. Flores-Prieto, "Nanofluids stability in flat-plate solar collectors: A review," *Sol. Energy Mater. Sol. Cells*, vol. 271, p. 112832, Jul. 2024. https://doi.org/10.1016/j.solmat.2024.112832

[15] J. Lei, Z. Luo, S. Qing, X. Huang, and F. Li, "Effect of surfactants on the stability, rheological properties, and thermal conductivity of Fe_3O_4 nanofluids," *Powder Technol.*, vol. 399, p. 117197, Feb. 2022. https://doi.org/10.1016/j.powtec.2022.117197

[16] K. Cacua, F. Ordoñez, C. Zapata, B. Herrera, E. Pabón, and R. Buitrago-Sierra, "Surfactant concentration and pH effects on the zeta potential values of alumina nanofluids to inspect stability," *Colloids Surf. A Physicochem. Eng. Asp.*, vol. 583, p. 123960, Dec. 2019. https://doi.org/10.1016/j.colsurfa.2019.123960

[17] M. Usman Sajid, and Y. Bicer, "Impacts of ultrasonication time and surfactants on stability and optical properties of CuO, Fe_3O_4, and CNTs/water nanofluids for spectrum selective applications," *Ultrason. Sonochem.*, vol. 88, p. 106079, Aug. 2022. https://doi.org/10.1016/j.ultsonch.2022.106079

[18] G. D. Gosavi, P. Sivamurugan, M. D. Shende, and A. D. Pingale, "Recent developments of sonication process in stability and efficiency of nanofluid-based coolants: A review," *Mater. Today Proc.*, Jul. 2023. https://doi.org/10.1016/j.matpr.2023.07.068

[19] S. Choi, R. Dev Mukhopadhyay, S. Kumar Sen, I. Hwang, and K. Kim, "Out-of-equilibrium chemical logic systems: Light- and sound-controlled programmable spatiotemporal patterns and mechanical functions," *Chem*, vol. 8, no. 8, pp. 2192-2203, Aug. 2022. https://doi.org/10.1016/j.chempr.2022.04.020

[20] H. Kim, J. Ham, N. You, G. Gim, and H. Cho, "Enhancing solar thermal energy harvesting efficiency and temperature uniformity of Fe_3O_4 nanofluid in receiver of direct solar thermal collector using dynamic magnetic field," *Appl. Therm. Eng.*, vol. 236, Part C, p. 121744, Jan. 2024. https://doi.org/10.1016/j.applthermaleng.2023.121744

[21] J. J. Alcalde-Castro, L. Álvarez-Gil, and A. Restrepo-Martínez, "Experimental Evaluation of Photothermal Conversion Magnetite Nanofluids under the Influence of Dynamic Magnetic Field," in *Optica Imaging Congr. 2024 (3D, AOMS, COSI, ISA, pcAOP) (2024),* p. FD1.8, Jul. 2024 https://doi.org/10.1364/ISA.2024.FD1.8

[22] M. M. Selim, S. El-Safty, A. Tounsi, and M. Shenashen, "Review of the impact of the external magnetic field on the characteristics of magnetic nanofluids," *Alex. Eng. J.*, vol. 76, pp. 75-89, Aug. 2023. https://doi.org/10.1016/j.aej.2023.06.018

[23] M. Talebian Gevari, T. Abbasiasl, S. Niazi, M. Ghorbani, and A. Koşar, "Direct and indirect thermal applications of hydrodynamic and acoustic cavitation: A review," *Appl. Therm. Eng.,* vol. 171, p. 115065, May. 2020. https://doi.org/10.1016/j.applthermaleng.2020.115065

[24] V. Rabiei Faradonbeh, S. Rabiei, H. Rabiei, M. Goodarzi, M. R. Safaei, and C. X. Lin, "Power-law fluid micromixing enhancement using surface acoustic waves," *J. Mol. Liq.*, vol. 347, p. 117978, Feb. 2022. https://doi.org/10.1016/j.molliq.2021.117978

[25] Y. Ou, Z. Liu, Y. Liu, L. Yan, and Z. Wen, "The flow field and convective heat transfer in the unit structure of heat exchangers by using acoustic waves," *Ann. Nucl. Energy*, vol. 205, p. 110587, Sep. 2024. https://doi.org/10.1016/j.anucene.2024.110587

[26] D. Zheng, J. Yao, H. Zhu, J. Wang, and C. Yin, "Optimizing photothermal conversion efficiency in a parabolic through direct absorption solar collector through ferrofluid and magnetic field synergy," *Energy Convers. Manag.*, vol. 285, p. 117020, Jun. 2023. https://doi.org/10.1016/j.enconman.2023.117020

[27] K. Guedri *et al.*, "Thermal analysis of ethylene glycol based tetra hybrid nanofluid flow over a stretchable permeable surface under the influence of induced magnetic field," *J. Mol. Liq.*, vol. 437, Part B, p. 128485, Nov. 2025. https://doi.org/10.1016/j.molliq.2025.128485

[28] I. Hwang *et al.*, "Audible sound-controlled spatiotemporal patterns in out-of-equilibrium systems," *Nat. Chem.*, vol. 12, no. 9, pp. 808-813, Sep. 2020. https://doi.org/10.1038/s41557-020-0516-2

[29] N. Heidari, M. Rahimi, and N. Azimi, "Experimental investigation on using ferrofluid and rotating magnetic field (RMF) for cooling enhancement in a photovoltaic cell," *Int. Commun. Heat Mass Transf.*, vol. 94, pp. 32-38, May. 2018. https://doi.org/10.1016/j.icheatmasstransfer.2018.03.010

[30] C. Li *et al.*, "A review on ultrasound-enhanced heat transfer," *Ultrasonics Sonochemistry*, vol. 121, p. 107570, Oct. 2025. https://doi.org/10.1016/j.ultsonch.2025.107570

[31] M. M. Sarafraz, V. Nikkhah, S. A. Madani, M. Jafarian, and F. Hormozi, "Low-frequency vibration for fouling mitigation and intensification of thermal performance of a plate heat exchanger working with CuO/water nanofluid," *Appl. Therm. Eng.*, vol. 121, pp. 388-399, Jul. 2017. https://doi.org/10.1016/j.applthermaleng.2017.04.083

[32] M. Dehbani, M. Rahimi, and Z. Rahimi, "A review on convective heat transfer enhancement using ultrasound," *Appl. Therm. Eng.*, vol. 208, p. 118273, May. 2022. https://doi.org/10.1016/j.applthermaleng.2022.118273

[33] K. B. Saleem, M. Omri, W. Aich, B. M. Alshammari, H. Rmili, and L. Kolsi, "Numerical Investigation of a Rotating Magnetic Field Influence on Free Convective CNT/Water Nanofluid Flow within a Corrugated Enclosure," *Mathematics*, vol. 11, no. 1, p. 18, Jan. 2023. https://doi.org/10.3390/math11010018

[34] C. Zhang *et al.*, "Acoustofluidics at Audible Frequencies—A Review," *Engineering*, vol. 44, pp. 51-72, Jan. 2025. https://doi.org/10.1016/j.eng.2024.03.020

[35] Y. Liu *et al.*, "Manipulation with sound and vibration: A review on the micromanipulation system based on sub-MHz acoustic waves," *Ultrason. Sonochem.*, vol. 96, p. 106441, Jun. 2023. https://doi.org/10.1016/j.ultsonch.2023.106441

[36] G. Shen, L. Ma, S. Zhang, S. Zhang, and L. An, "Effect of ultrasonic waves on heat transfer in Al2O3 nanofluid under natural convection and pool boiling," *Int. J. Heat Mass Transf.*, vol. 138, pp. 516-523, Aug. 2019. https://doi.org/10.1016/j.ijheatmasstransfer.2019.04.071

CONFLICT OF INTEREST

The authors declare that they have no conflict of interest.

AUTHORSHIP CONTRIBUTION

Juan José Alcalde-Castro: Conceptualization, Methodology, Formal analysis, Investigation, Original Draft Writing, Review & Editing, Visualization.

Laura Álvarez-Gil: Conceptualization, Methodology, Formal analysis, Investigation, Data curation, Original Draft Writing, Review & Editing, Visualization, Supervision.

Alejandro Restrepo-Martínez: Conceptualization, Methodology, Formal analysis, Original Draft, Review & Editing, Supervision.